European Journal of Obstetrics & Gynecology and Reproductive Biology 144S (2009) S170–S178

Contents lists available at ScienceDirect

European Journal of Obstetrics & Gynecology and Reproductive Biology

journal homepage: www.elsevier.com/locate/ejogrb

The effects of the ovarian cycle and pregnancy on uterine vascular impedance and uterine artery mechanics

Benjamin J. Sprague [a,b], Terrance M. Phernetton [b], Ronald R. Magness [b,c,d], Naomi C. Chesler [a,*]

[a] Department of Biomedical Engineering, University of Wisconsin, Madison, WI, USA
[b] Department of Ob/Gyn Perinatal Research Laboratories, University of Wisconsin, Madison, WI, USA
[c] Department of Animal Sciences, University of Wisconsin, Madison, WI, USA
[d] Department of Pediatrics, University of Wisconsin, Madison, WI, USA

ARTICLE INFO

Keywords:
Estrogen
Progesterone
Uterine vascular resistance
Circumferential elastic modulus

ABSTRACT

Objectives: Uterine vascular resistance (UVR) is the ratio of systemic mean arterial pressure to mean uterine blood flow and is sensitive to changes in small arteries and arterioles. However, it provides little or no insight into changes in large, conduit arteries. Fluctuations in estrogen (E2) and progesterone (P4) levels during the ovarian cycle are thought to cause uterine resistance artery vasodilation; the effects on large arteries are unknown. Herein, our objective was to use the uterine vascular impedance, which is sensitive to changes in small and large arteries, to determine the effects of the ovarian cycle and pregnancy on the entire uterine vasculature.

Study design: Uterine vascular perfusion pressure and flow rate were recorded simultaneously in anesthetized sheep in the nonpregnant (NP) luteal (NP-L, $n = 6$) and follicular (NP-F, $n = 7$) phases and in late pregnancy (CP, $n = 10$). Impedance and metrics of impedance (input impedance Z_0, index of wave reflection R_W, characteristic impedance Z_C) were calculated. E2 and P4 levels were measured from jugular vein blood samples. Finally, from pressure-diameter tests post-mortem, large uterine artery circumferential elastic modulus (E_{Circ}) was measured. Significant differences were evaluated by two-way ANOVA or Student's *t*-test.

Results: As expected, E2:P4 was higher in the NP-F group compared to the NP-L group ($p < 0.05$). Also as expected, UVR and Z_0 decreased in the follicular phase compared to the luteal ($p < 0.05$), but R_W, Z_C, and E_{Circ} were unaltered. Pregnancy not only substantially decreased UVR (and Z_0) ($p < 0.00001$) but also decreased Z_C ($p < 0.001$), R_W ($p < 0.0001$), E_{Circ} ($p < 0.01$), and pulse wave velocity ($p < 0.0001$).

Conclusions: The E2:P4 ratio mediates resistance artery vasodilatation in nonpregnant states, but has no effect on conduit artery size or stiffness. In contrast, pregnancy causes dramatic vasodilation and remodeling, including substantial reductions in conduit artery stiffness and increases in conduit artery size, which affect pulsatile uterine hemodynamics.

1. Introduction

In contrast to the vascular resistance, which measures the opposition to mean or steady flow in a vascular network, vascular impedance measures the opposition to pulsatile flow. Since nearly all blood flow in the body is pulsatile in nature, impedance reflects the true work required to perfuse a vascular bed. Also, since the mean flow is a component of any pulsatile flow, resistance can be directly obtained from the frequency-dependent impedance spectrum. Indeed, 0 Hz impedance measured *in vivo* is equivalent to the vascular resistance distal to the point-of-measure. Moreover, impedance yields other useful metrics of circulatory function such as the characteristic impedance (Z_C), which provides insight into arterial size and stiffness, and index of wave reflection (R_W), which reflects the effects of taper, branches and changes in arterial stiffness on pressure and flow waveforms [1]. Finally, impedance inherently contains more information than resistance, which may be useful in diagnosing vascular bed abnormalities such as may occur with infertility or in preeclampsia with and without intrauterine growth retardation. However, the changes in uterine vascular impedance that occur during the ovarian cycle and with healthy pregnancies have not been reported.

The ovarian cycle is characterized by fluctuations in the sex hormones estrogen (E2) and progesterone (P4) [1]. The luteal

* Corresponding author at: Department of Biomedical Engineering, University of Wisconsin at Madison, 2146 Engineering Centers Building, 1550 Engineering Drive, Madison, WI 53706-1609, USA. Tel.: +1 608 265 8920; fax: +1 608 265 9239.
E-mail address: chesler@engr.wisc.edu (N.C. Chesler).

0301-2115/$ – see front matter © 2009 Elsevier Ireland Ltd. All rights reserved.
doi:10.1016/j.ejogrb.2009.02.041

phase is a time of relatively low E2 and high P4 whereas the follicular phase, in which the uterus is readied for implantation, is a time of higher E2 and lower P4 [2–4]. Increased E2:P4 is known to increase mean blood flow to many vascular beds, especially the uterus [2,5–16]. Local, exogenous treatment with E2 can also increase blood flow to the uterine vascular bed [9,12,16]. Since blood pressure does not change significantly over the ovarian cycle, these increases in blood flow are enabled by a drop in UVR, presumably by arteriolar vasodilation. Changes in large artery size and stiffness over the ovarian cycle have not been investigated to our knowledge. Furthermore, changes in pulsatile uterine hemodynamics over the ovarian cycle, which would be a consequence of altered large artery structure and function, have not been reported.

In healthy pregnancies, uterine blood flow increases by 20–50-fold with little to no change in perfusion pressure [10,14,17–19]; thus, uterine vascular resistance (UVR) typically decreases 20–50-fold. This dramatic drop is enabled in part by the physiological transformation of resistance-sized arteries into the uteroplacental bed [20–24] and also by large uterine artery remodeling [20–25]. In particular, in healthy pregnancies large uterine arteries grow in diameter nearly 2-fold and become less stiff [20–26]. Nevertheless, changes in pulsatile uterine hemodynamics with pregnancy are not typically reported.

The goals of this study were to determine the effects of the ovine ovarian cycle and healthy pregnancy on uterine vascular impedance, and the dependence of impedance changes on large, conduit uterine artery structure and function changes. We hypothesized that UVR and input impedance would decrease during the follicular phase in response to the increased E2:P4 ratio, but that changes in conduit arteries would be minimal. In addition, we hypothesized that pregnancy would result in dramatically decreased UVR (by 20–50-fold) as well as increased large artery diameter and decreased large artery stiffness, characteristic impedance, wave reflections and pulse wave velocity (PWV). Finally, we investigated the effects of the ovarian cycle and healthy pregnancy on the clinically used blood flow indices systolic to diastolic ratio (S/D), resistivity index (RI) and pulsatility index (PI).

2. Materials and methods

2.1. Animal preparation

Procedures for animal handling and protocols for experimental procedures were approved by the University of Wisconsin-Madison Research and Animal Care and Use Committees of both the Medical School and the College of Agriculture and Life Sciences. This study contained three groups of multiparous female sheep of mixed western breeds: two nonpregnant (NP) groups synchronized to different phases of the ovarian cycle and one late-gestation, pregnant group. The NP animals ($n = 13$) were experimentally synchronized to be sacrificed during two distinct and controlled points of the ovarian cycle, i.e. the late follicular phase during the periovulatory period (NP-F, $n = 7$) and the late luteal phase 10–11 days post-ovulation (NP-L, $n = 6$), as previously described [2]. Briefly, controlled internal drug-releasing devices (CIDRs) were placed vaginally to deliver luteal phase levels of progesterone for 9–11 days. Upon removing the CIDR, injections of prostaglandin F2 alpha (7.5 mg Lutalyse) and pregnant mare serum gonadotropin (PMSG) (500 IU) were given IM. The late follicular/periovulatory and luteal phases were defined as 48 h and 12–13 days post-CIDR removal and injections, respectively. Pregnant animals were studied as a positive control of (expected) significant changes in large artery mechanics. The control pregnant group (CP, $n = 10$) was studied at 120–130 days gestation. The natural gestation length for sheep is 145–147 days.

2.2. Hemodynamic measurements

During non-survival surgery just prior to sacrifice, animals were anesthetized with pentobarbital sodium (Nembutal; 50 mg/ml) via a jugular vein catheter. Then, in the supine position, uterine artery pressure was measured with a fluid filled catheter inserted via cannulation of the saphenous branch of the femoral artery and advanced to the level of the internal iliac, near the origin of the uterine artery [11,15]. Heart rate (HR) was also measured from this pressure waveform. Following a midventral incision, the primary uterine arteries supplying each horn of the uterus in the mesometrium were identified and isolated. Uterine blood flow in one of these arteries (i.e., unilateral) was measured using a cuff-type ultrasonic flow probe. Depending on the size of the artery, 3 or 6 mm ultrasound probes (3RS and 6RS probes, Transonic Systems Inc., Ithaca, NY) were used. Pressure and flow measurements were sampled simultaneously at 120 Hz using WinDaq Pro Data Acquisition software (DATAQ Instruments, Akron, OH) [11,15].

2.3. Hemodynamic analyses

Pressure and flow waveforms for ten sequential cardiac cycles were isolated and independently analyzed. UVR was calculated as mean systemic arterial pressure (P_{Mean}) divided by mean uterine blood flow (Q_{Mean}):

$$\mathrm{UVR} = \frac{P_{Mean}}{Q_{Mean}} \quad (1)$$

This equation is equivalent to the more traditional definition of resistance as mean pressure difference across a vascular bed divided by mean flow through the vascular bed if the downstream (uterine venous) pressure is close to zero or constant over the ovarian cycle and with pregnancy, which is typically assumed for the uterine venous bed (~1–2 mmHg).

To calculate input impedance in the frequency domain, each cardiac cycle underwent processing to eliminate signal noise that included applying a Hann window and zero-padding (MATLAB, The MathWorks Inc., Natick, MA). These processed waveforms were then resolved into their frequency components using a discrete fast Fourier transform function (MATLAB) and their ratio taken at all harmonics of the heart rate as previously described [27–29]. Here we present only impedance magnitude because the distance between the sites of pressure and flow measurement made the impedance phase calculation an unreliable measure of pressure–flow lag without additional calibration studies. Furthermore, the impedance phase contains less information than the impedance magnitude [30].

Several metrics of the input impedance were calculated. The input resistance (Z_0) was calculated as the input impedance magnitude at 0 Hz.

$$Z_0 = Z(f = 0\,\mathrm{Hz}) \quad (2)$$

Characteristic impedance, Z_C, was calculated as the average impedance magnitude for all frequencies above the first minimum of each impedance spectrum [28].

$$Z_C = \left\langle Z(f > f_{\min(Z)}) \right\rangle \quad (3)$$

Finally, the index of wave reflection, R_W, was computed as in [30]:

$$R_W = \frac{Z_0 - Z_C}{Z_0 + Z_C} \quad (4)$$

Coefficients of variation for these impedance metrics over the ten cycles of data collected for each animal were less than 8%; the average value was used for each animal.

Clinically used indices of blood flow, S/D, RI and PI, were calculated using the peak systolic flow (Q_{Sys}), end-diastolic flow (Q_{Dia}), and mean uterine blood flow Q_{Mean} as in [31]:

$$\frac{S}{D} = \frac{Q_{Sys}}{Q_{Dia}}$$

$$RI = \frac{Q_{Sys} - Q_{Dia}}{Q_{Sys}} \quad (4)$$

$$PI = \frac{Q_{Sys} - Q_{Dia}}{Q_{Mean}}$$

2.4. Estrogen and progesterone measurements and analyses

Jugular vein blood samples were collected into vials containing ethylene diamine tetraacetic acid (EDTA) and centrifuged for isolation of blood plasma. Blood plasma was stored frozen (−20 °C) until 17-β estradiol (E2) and progesterone (P4) hormone levels were analyzed. To analyze E2, plasma (400 μl) was extracted with diethyl ether and concentrations of E2 were evaluated by RIA as previously reported [2,3,32]. Plasma P4 was analyzed using the commercial Coat-A-Count RIA kit from Diagnostic Products Corporation (DPC, Los Angeles, CA). All samples were analyzed in duplicate and in a single assay (intra-assay percent relative standard deviations were 3.9% for E2 and 11.2% for P4).

2.5. Large uterine artery mechanical measurements

After hemodynamic data and blood samples were obtained, animals were euthanized and the uterus was removed. The uterine arterial tree was dissected from each (right and left) uterine horn. In each excised arterial tree, one primary, two secondary and at least four tertiary (third generation) arteries were obtained intact. One secondary artery from each horn (right and left) was randomly selected for mechanical testing and placed in a cold (4 °C) Ca^{2+}-free, KREBS + HEPES solution (composition (mM): NaCl 144; KCl 5.9; $MgCl_2$ 1.2; glucose 11; Hepes 10; pH 7.4) with 0.1 mM EGTA (Ethylene glycol-bis-(2-aminoethyl)-N,N,N′,N′-tetraacetic acid) to ensure fully relaxed smooth muscle cells.

For mechanical testing, one end of each artery was cannulated with polyvinyl tubing with an outer diameter between 1.5 and 2.5 mm. The Ca^{2+}-free, KREBS + HEPES solution with 0.1 mM EGTA was heated to 37 °C and used as both perfusate and superfusate. The other end and all side branches of the artery were tied off. No initial stretch was imposed; the artery was provided no anchoring in the longitudinal direction but allowed to expand freely. After an initial equilibration period (30 min), intraluminal pressure was increased from 0 to 120 mmHg in a stair-step manner in 10 mmHg increments. The isolated artery was digitally photographed at 12× magnification to obtain the pressure-dependent outer diameter (OD_p) and axial length (L_p) via externally visible landmarks on the artery segments in each loaded state. The OD and length measurements taken at zero transmural pressure were used as a reference state (OD_0 and L_0, respectively).

Following the stair-step pressurization tests, arteries were fixed at approximate *in vivo* pressure (85–95 mmHg) [10–12,15,33,34] with 4% formalin solution for at least 2 h. Outer diameter and length were measured post-fixation (OD_f and L_f, respectively). To measure inner diameter and wall thickness post-fixation at the *in vivo* pressure (ID_f and WT_f, respectively), three to four rings were cut from the fixed tissue in 0.25–0.35 mm lengths. These sections were then digitally photographed in cross-section. Inner and outer circumferences were measured for each ring and used to calculate inner and outer diameter, respectively, assuming circular cross-sections (ID_f and $OD_{f,ring}$, respectively). WT_f was calculated as follows:

$$WT_f = \frac{OD_{f,ring} - ID_f}{2} \quad (6)$$

The agreement between OD_f and $OD_{f,ring}$ served as a useful check on the measurement integrity.

Image analysis software (MetaVue, Molecular Devices, Downington, PA) calibrated to scales on each image were used to make all measurements from digital photographs.

2.6. Large uterine artery mechanical analyses

In order to calculate uterine artery elastic modulus, circumferential stress and strain at each pressure step were calculated. First, circumferential Green strain (ε_{Circ}) was calculated based on stretch from the zero pressure state:

$$\lambda_{Circ} = \frac{OD_p}{OD_0} \qquad \varepsilon_{Circ} = \frac{1}{2}(\lambda_{Circ}^2 - 1) \quad (7)$$

Then, inner diameter at each pressure (ID_p) was calculated from the fixed dimensions assuming conservation of volume:

$$ID_p = \sqrt{\frac{L_f}{L_p}(OD_f^2 - ID_f^2) + OD_p^2} \quad (8)$$

Cauchy circumferential stress (σ_{Circ}) at the inner wall surface was calculated using a thick-walled assumption because the ratio of ID_p/WT_p was less than 20 for most pressures:

$$\sigma_{Circ} = \frac{P(OD_p^2 + ID_p^2)}{OD_p^2 - ID_p^2} \quad (9)$$

where P is the transmural pressure at which OD_p and ID_p were measured. Finally, circumferential incremental elastic modulus (E_{Circ}) was calculated as the slope of the circumferential stress versus circumferential strain relationship over a physiological pressure range.

Also, uterine artery PWV was approximated using the Moens–Korteweg equation for a thick-walled vessel based on the fixed dimensions:

$$c_0 = \frac{E_{Circ}(OD_f^2 - ID_f^2)}{3\rho OD_f^2} \quad (10)$$

where ρ is the density of blood (1.06 g/cm^3).

2.7. Statistical analysis

All results are expressed as mean ± S.E. Significance of the differences between the various groups was evaluated by two-way ANOVA or Student's *t*-test. The results were considered statistically significant when $p < 0.05$.

3. Results

3.1. Estrogen and progesterone measurements and analyses

The ratio of 17-β estradiol (E2) to progesterone (P4) in systemic plasma was higher in NP-F compared to NP-L animals ($p < 0.05$), primarily as a result of very low levels of P4. NP-F animals tended to have higher levels of E2, but this difference did not reach statistical significance ($p > 0.05$) because one animal showed an ovarian structure identified as a corpus hemmoragicum that was consistent with recent ovulation, i.e. after E2 has peaked and is falling. As we have reported previously [2–4], the hormone profiles found here were consistent with the observed

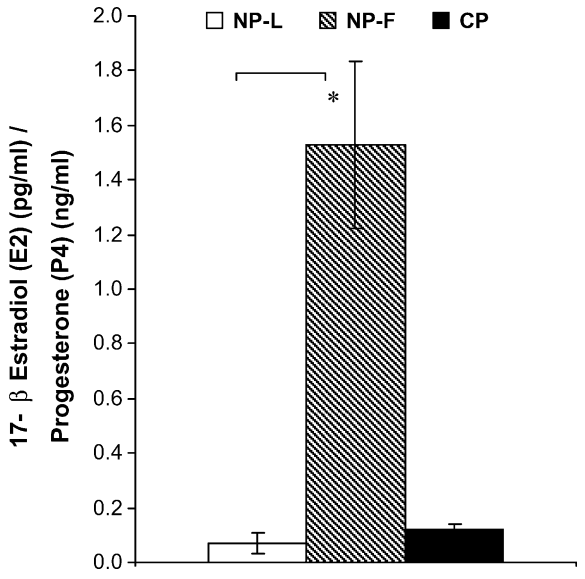

Fig. 1. The ratio of 17-β estradiol (E2) to progesterone (P4) within plasma in jugular vein blood samples obtained from NP-L, NP-F and CP animals. Compared to NP-L, the E2:P4 ratio increased in NP-F ($^*p < 0.05$). In pregnancy, elevated levels of both E2 and P4 returned the E2:P4 ratio to approximately NP-L levels. Data are means ± S.E.

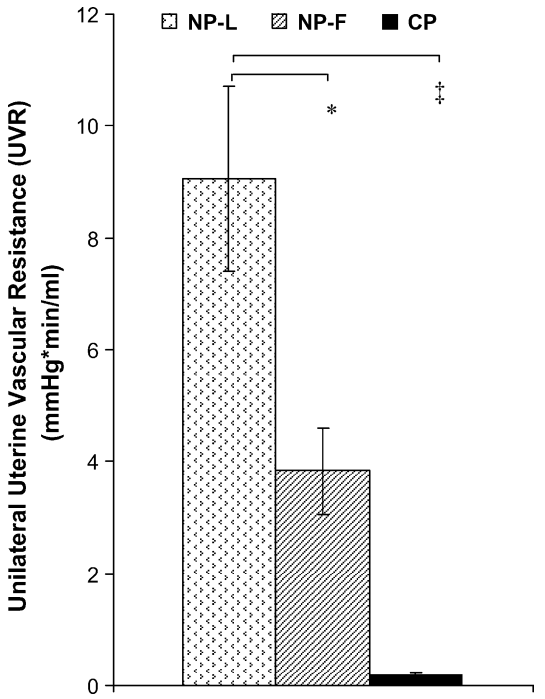

Fig. 2. Unilateral uterine vascular resistance (UVR) of NP-L, NP-F and CP animals. UVR was computed as P_{Mean} divided by Q_{Mean} in one uterine artery (hence, unilateral). Compared to NP-L, UVR decreased by over 2-fold in NP-F ($^*p < 0.05$) and over 20-fold in CP ($^‡p < 0.00001$). Data are means ± S.E.

size and appearance of the ovarian follicular and luteal structures in NP ewes (data not shown). In the pregnant sheep, levels of E2 and P4 were both approximately 10-fold greater than in the NP-L animals, leading to no difference between these groups in E2:P4 ratio (Fig. 1).

3.2. Hemodynamic measurements and analyses

As expected, blood flow increased 2-fold in NP-F animals compared to NP-L ($p < 0.05$), and increased 20-fold in CP animals compared to NP-L ($p < 0.00001$) (Table 1). No differences in measured pressures (P_{Mean}, P_{Sys} and P_{Dia}) or HR were observed (Table 1). Therefore, the calculated decreases in UVR in the NP-F and CP groups (Fig. 2) were solely due to increases in blood flow.

The impedance magnitude at 0 Hz, Z_0, for each group was identical to the UVR, as expected, which served as a useful check on the calculation. As noted above, the calculation of Z_C was based on the average impedance magnitude above the first minimum, $f_{min(Z)}$ [28]; NP-F and CP animals tended to have a greater $f_{min(Z)}$ (5.0–6.0 Hz) compared to NP-L (4.5–5.5 Hz), but the differences were not statistically significant (data not shown). Z_C decreased in CP animals compared to NP-L and NP-F ($p < 0.001$); Z_C tended to be lower in NP-F animals compared to NP-L, but the difference did not reach statistical significance (Fig. 3A). The index of wave reflection, R_W, also decreased in CP animals compared to NP-L and NP-F animals ($p < 0.001$), and was not different between NP-L and NP-F animals (Fig. 3B).

None of the clinically used blood flow indices were affected by the ovarian cycle. However, pregnancy substantially decreased the S/D ratio, RI and PI ($p < 0.001$) (Fig. 4).

3.3. Large uterine artery mechanical measurements and analyses

Inner diameter and outer diameter fixed at *in vivo* pressures (ID_f and OD_f, respectively) increased in CP animals compared to NP-L and NP-F ($p < 0.00001$ for ID_f and OD_f for both groups). Wall thickness at fixed at *in vivo* pressures (WT_f) remained unchanged throughout the ovarian cycle and with pregnancy (Table 2). E_{Circ} was not different between NP-L and NP-F groups but was significantly lower in CP animals than NP-L ($p < 0.01$) (Fig. 5). Similarly, PWV decreased in CP animals compared to NP-L ($p < 0.0001$), but was not different between NP-L and NP-F groups (Fig. 6).

4. Discussion

The major findings of this study are that measurements of uterine vascular impedance are able to detect significant resistance artery vasodilation mediated by the E2:P4 ratio during the ovine ovarian cycle, and do not show evidence of altered conduit artery size or stiffness via changes in metrics of impedance. In contrast,

Table 1
Heart rate (HR), mean, systolic and diastolic blood pressure (P_{Mean}, P_{Sys} and P_{Dia}, respectively) and mean, systolic and diastolic blood flow (Q_{Mean}, Q_{Sys} and Q_{Dia}, respectively) for NP-L, NP-F and CP animals. HR and blood pressure did not vary between groups. Compared to NP-L animals, blood flow increased in NP-F and CP animals.

	HR (bpm)	P_{Mean}	P_{Sys}	P_{Dia}	Q_{Mean}	Q_{Sys}	Q_{Dia}
NP-L	145 ± 7.8	143 ± 21.1	170 ± 23.2	126 ± 19.1	17.5 ± 1.9	27.6 ± 2.9	10.0 ± 1.5
NP-F	136 ± 6.0	120 ± 6.5	140 ± 7.0	108 ± 6.2	38.0 ± 7.2*	60.3 ± 11.4*	20.4 ± 5.7*
CP	134 ± 4.8	138 ± 13.0	161 ± 15.1	122 ± 11.7	813 ± 73.2‡	1070 ± 100‡	610 ± 53.1‡

Data are means ± S.E. All flow measurements were made in the primary artery of one uterine horn (i.e., unilaterally).
* Indicates significant difference between NP-F and NP-L ($p < 0.05$).
‡ Indicates significant difference between CP and NP-L ($p < 0.00001$).

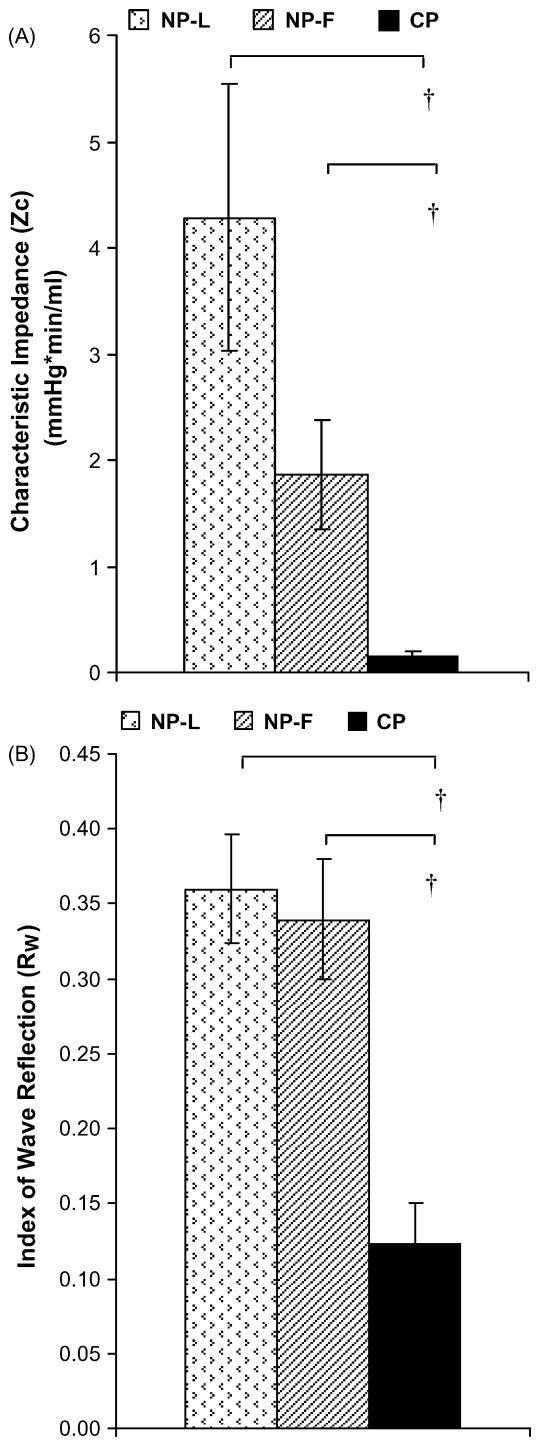

Fig. 3. Metrics of uterine vascular impedance from NP-L, NP-F and CP animals. (A) Characteristic impedance (Z_C) decreased in CP animals compared to NP-L and NP-F ($^{\dagger}p < 0.001$); (B) R_W also decreased in CP compared to NP-L and NP-F animals ($^{\dagger}p < 0.001$). Data are means ± S.E.

uterine vascular impedance metrics Z_0 (equivalent to UVR), Z_C and R_W are all significantly affected by normal pregnancy, as are conduit artery size, elastic modulus and pulse wave velocity as well as clinically used blood flow indices. Overall, these results demonstrate that uterine vascular impedance is a useful tool for detecting changes, and possibly abnormalities, in conduit and resistance artery structure and function over the ovarian cycle and with pregnancy.

4.1. Systemic levels of estrogen and progesterone

The ratio of E2 to P4 previously has been shown to increase dramatically during the follicular phase of the ovine ovarian cycle [2,3,7,35]. In addition, E2 and P4 levels have been shown to increase several-fold during pregnancy and maintain an E2:P4 ratio equivalent to the luteal phase of the ovarian cycle [2,3,7,35,36]. The results of the present study are in agreement with the prior literature.

4.2. Hemodynamic measurements and analyses

P_{Mean} and HR have been reported not to change with the ovarian cycle [15,37–39], as found herein. In late gestation pregnant sheep, however, P_{Mean} and HR have been found to decrease [10–12,15,16,34]. Our measurements of P_{Mean} and HR did not decrease with pregnancy and indeed were elevated from those measured previously in unanesthetized, standing (non-supine position) [10–12,15,16,34]. Additional studies by our group suggest that these differences are due to the combined effects of posture (supine vs. standing) and anesthesia (data not shown).

The 2-fold decrease in UVR from the luteal phase (NP-L) to the follicular phase (NP-F) is most likely related to estrogen-mediated vasodilation. As noted above, we found that the ratio of E2 to P4 increased during the follicular phase; in prior work, the ratio of E2 to P4 has been shown to cause vasodilation, especially in the uterine vascular bed [2,9–11,16,40–42]. The likely mechanism by which increases in E2:P4 decrease resistance is via increased production of the potent endogenous vasodilator nitric oxide. Prior data from our group have shown that vasodilation *in vivo* is initiated by a rise in nitric oxide production that is mediated by endothelial estrogen receptors [2,15]. In CP animals, the E2:P4 was equivalent to luteal phase levels whereas UVR was nearly 20-fold lower. Thus, E2:P4 was not a predictor of UVR despite the similar E2:P4 values. In pregnancy, it is well known that resistance-sized arteries are transformed into the uteroplacental bed [21,41,43,44], which is largely independent of E2:P4 during late gestation. This uterine vascular transformation is likely the dominant mechanism by which UVR decreases with pregnancy.

Vascular impedance measurements enable the characteristics of more proximal (to point-of-measure) arteries to be distinguished from those of more distal vessels. In addition, impedance offers a more complete description of the hemodynamic work required to perfuse a vascular bed than the more commonly used resistance. One disadvantage of impedance is that the full frequency-dependent magnitude and phase spectra are required for a complete understanding of pressure–flow relationships. However, if one is only interested in large artery size and stiffness and wave reflections at the vascular bed origin, metrics of impedance based only on the magnitude can be useful. Herein we investigated the effects of the ovarian cycle and pregnancy on two metrics of impedance that give insight into large, conduit artery characteristics: Z_C and R_W.

Measurements of uterine vascular characteristic impedance changes during the ovarian cycle have not been previously reported. Characteristic impedance Z_C is directly proportional to proximal (to point-of-measure) arterial stiffness and inversely proportional to proximal arterial inner diameter. Stiffness, in turn, is proportional to elastic modulus and wall thickness and inversely related to inner diameter [45]. During the follicular phase, Z_C tended to decrease, although not significantly, which suggests a small increase in inner diameter since no change in elastic modulus was found (Fig. 5). In contrast, with pregnancy, Z_C decreased significantly (Fig. 3A), which is explained by the significant decrease in large artery elastic modulus (Fig. 5).

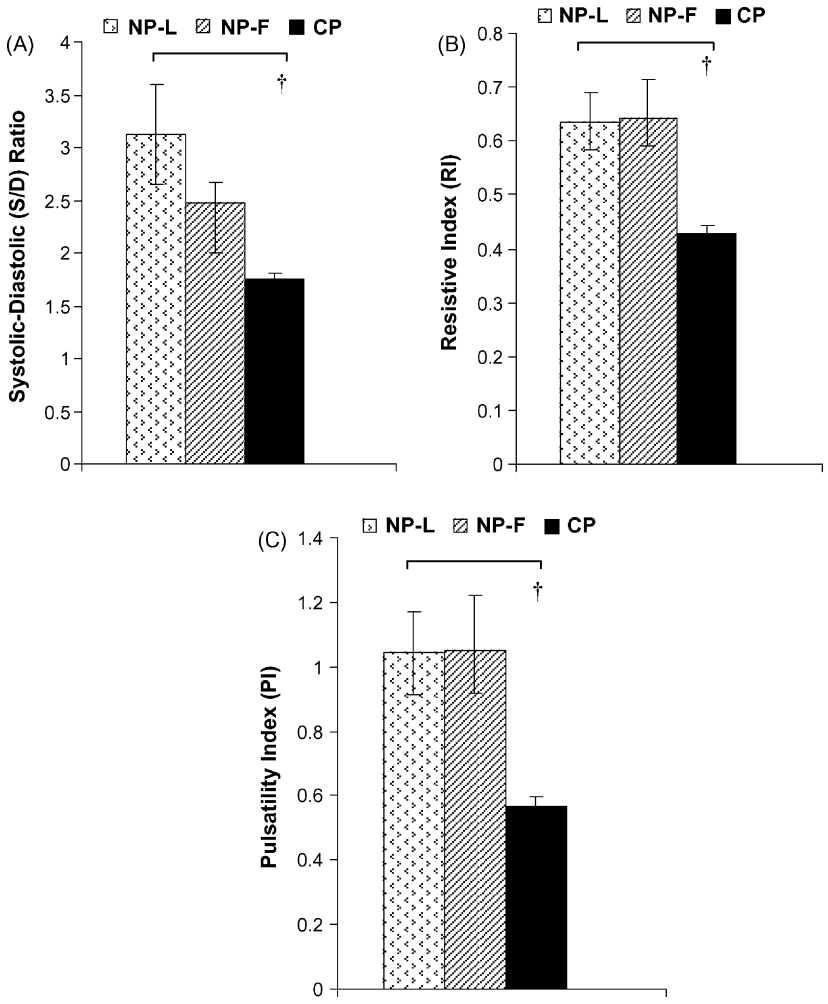

Fig. 4. Three indices of blood flow pulsatility used clinically, systolic-to-diastolic ratio (S/D), resistive index (RI), and pulsatility index (PI), computed for NP-L, NP-F and CP animals. No differences were seen in (A) S/D, (B) RI and (C) PI between NP-L and NP-F animals. In contrast, all three showed reductions with pregnancy compared to NP-L ($^{\dagger}p < 0.001$), which indicates decreased blood flow pulsatility. Data are means ± S.E.

Measurements of wave reflection at the entrance to the uterine vascular bed during the ovarian cycle also have not been previously reported. The index of wave reflection R_W reflects mismatch between proximal and distal (conduit and resistance, respectively) artery impedance. Here we found that R_W remained unchanged between the luteal and follicular phases of the ovarian cycle (Fig. 3B). This is an interesting finding given the statistically significant decrease in downstream resistance. That is, the small but not significant decrease in Z_C coupled with the significant decrease in UVR (and thus Z_0) was sufficient to normalize R_W. This finding suggests that small increases in conduit artery inner diameter maintain pulse wave reflection at a constant level during the ovarian cycle.

Table 2
Inner diameter, outer diameter and wall thickness measured from secondary uterine arteries fixed at *in vivo* pressures (ID_f, OD_f and WT_f, respectively). With pregnancy, ID and OD were increased compared to NP-L and NP-F groups.

	ID_f (mm)	OD_f (mm)	WT_f (mm)
NP-L	1.27 ± 0.21	1.94 ± 0.24	0.34 ± 0.04
NP-F	1.58 ± 0.12	2.50 ± 0.09	0.42 ± 0.06
CP	3.37 ± 0.15‡,†	3.99 ± 0.22‡,†	0.33 ± 0.02

Data are means ± S.E.
† Indicates significant difference between CP and NP-F ($p < 0.001$).
‡ Indicates significant difference between CP and NP-L ($p < 0.00001$).

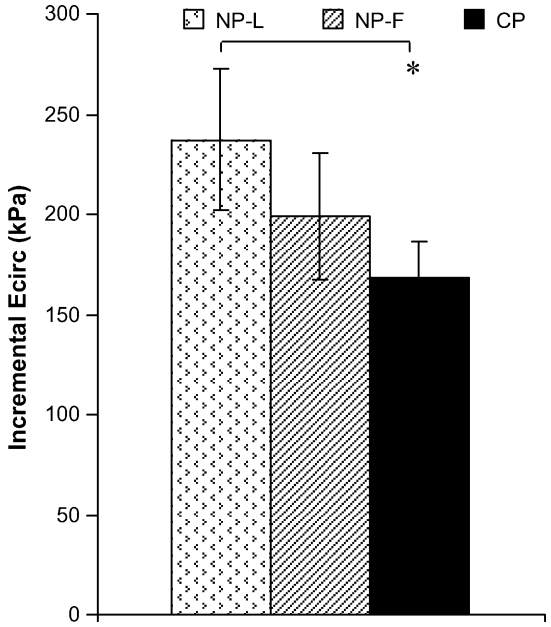

Fig. 5. Circumferential elastic modulus of large uterine arteries from NP-L, NP-F and CP animals. E_{Circ} did not change with the ovarian cycle (NP-L vs. NP-F) but was decreased in CP animals compared to NP-L animals ($^{*}p < 0.05$). Data are means ± S.E.

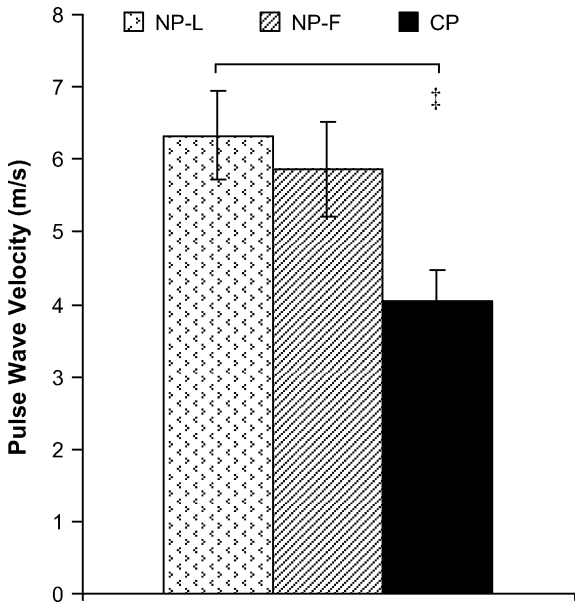

Fig. 6. Pulse wave velocity (PWV) within large uterine arteries calculated from uterine artery circumferential elastic modulus and diameter for NP-L, NP-F and CP animals. No differences were observed between NP-L and NP-F animals. PWV decreased with pregnancy ($^{\dagger}p < 0.001$). Data are means ± S.E.

It is noteworthy that wave reflection during pregnancy was almost zero. The spiral arteries in women and terminal caruncular-placentomal arteries in sheep are intrinsically transformed into the uteroplacental bed with pregnancy [21,41,43,44,46]. Since the muscular integrity of these arteries essentially disappears with pregnancy, and since wave reflections also nearly disappear with pregnancy, these arteries are likely a significant source of wave reflections in the nonpregnant uterus.

Clinically, the pulsatility of uterine blood flow is characterized via non-invasive measurements of instantaneous systolic and diastolic flow. Blood flow indices, including S/D, RI and PI, are able to detect reactivity to vasodilators [47–49] and improper uterine perfusion associated with preeclampsia when used in combination with other features of the blood flow waveform [50–53]. However, changes in clinically used uterine blood flow indices during the ovarian cycle in sheep have not been previously reported. Some differences between the ovarian cycle of humans and sheep are important to consider here. The ovine ovarian cycle is approximately 15–17 days, with a relatively short (48–56 h) follicular phase, the latter being periovulatory. In women, a longer follicular phase (~10–14 days), including a menstrual period at its beginning, extends the human ovarian cycle to approximately 28–30 days. During this prolonged follicular phase in humans, estrogen levels rise slowly, reaching very high levels close to ovulation, and then fall. The follicular phase in humans is largely a time of rising (but still lower than in the luteal phase) ovarian E2 production, because unlike the ovine model the human corpus luteum produces significant levels of estrogen. Because of this difference in ovine ovarian versus human menstrual cycle, it maybe more correct to compare clinical blood flow index results in the follicular phase in ewes to the late-follicular stage of the human just around the time of ovulation.

From the early- or mid-follicular to luteal phase in women, uterine blood flow increases and RI and PI decrease [54,55]. In our studies in sheep, no changes in S/D, RI or PI were observed between NP-L and NP-F. We suggest that the lack of change in these indices in ewes is due to the shorter follicular phase compared to the human. The significant decreases in S/D, RI and PI in pregnant sheep are consistent with the literature in humans [19,50,56,57] and suggest significant decreases in blood flow pulsations.

4.3. Uterine artery mechanical measurements and analyses

Uterine artery outer diameter, wall thickness and circumferential incremental elastic modulus did not vary over the ovarian cycle. It is important to note that these measurements were made in arteries with no smooth muscle cell tone. Certainly changes in tone over the ovarian cycle, possibly mediated by estrogen and the E2:P4 ratio, could alter large uterine artery diameter, wall thickness and elastic modulus. However, expected consequences of the possible changes in structure and function were not evident in the uterine vascular impedance measurements discussed above. Thus, we expect that the impact of the ovarian cycle on smooth muscle cell tone in large uterine arteries is minimal. Another limitation of these results is that they may have limited applicability to other species, such as the human, with longer follicular phases; i.e. the 48-h follicular periovulatory phase of the sheep may be too short for changes in structure and function to occur other than by changes in smooth muscle cell tone.

The 2-fold increase in OD and 2-fold decrease in E_{Circ} with pregnancy are in agreement with studies in other species [20–22,24]. There exists in the literature only one study using the sheep model to investigate the effects of pregnancy on the mechanics of large uterine arteries [25]. In contrast to the data in all other species and the results we report herein, Griendling et al. found that uterine artery elastic modulus increased with pregnancy [25]. However, it is important to note a methodological difference. We calculated elastic modulus as the slope of the stress–strain relationship in a physiological pressure range, whereas Griendling et al. calculated an incremental elastic modulus as a function of pressure [25]. These different methods can lead to different conclusions especially under conditions of large strain (approaching 100%). In terms of interpretation, both our data and the data by Griendling et al. show that the pregnant arteries have a larger change in diameter for an increment in pressure than the nonpregnant arteries. Thus, the pregnant arteries are less stiff.

Clinical studies have measured wave speed in systemic arteries over the human menstrual cycle and did not report any changes [38,39]. For example, Hayashi et al. found that PWV in the carotid-to-femoral artery was 5.4 m/s (S.D. 0.6) in the follicular phase and also 5.5 (S.D. 0.8) in the luteal phase [38,39]. Ounis-Skali found higher velocities in the femoral artery but still no differences over the ovarian cycle (8.13 S.D. 0.91 m/s vs. 7.85 S.D. 0.79 m/s for follicular vs. luteal) [40]. The PWVs found here in the uterine artery were in this same range in the follicular and luteal phases and also did not vary between over the ovarian cycle. However, we note that smooth muscle cell tone could vary over the ovarian cycle and alter PWV. All measurements on which the PWV calculation is based were made in the absence of smooth muscle cell tone. With pregnancy, the increase in OD and decrease in E_{Circ} resulted in a dramatically decreased PWV, to about 4 m/s. The combination of decreased pulse wave velocity and decreased wave reflections with pregnancy emphasizes the increased conduit function of the uterine vasculature during pregnancy. That is, these data suggest that the proximal and distal vasculature remodel and transform, respectively, during pregnancy to allow maximally increased blood flow to the fetus.

In summary, uterine vascular impedance is a useful measurement with which the effects of physiological or pathological changes in the uterine vasculature can be investigated. The combination of impedance and arterial mechanics data presented here strongly supports the effect of changes in the E2:P4 ratio during ovarian cycle on the uterine resistance arteries but not uterine conduit arteries. With pregnancy, both resistance and

conduit arteries are significantly altered and these structural and functional changes in the vasculature affect uterine vascular pressure–flow relationships. Finally, our data suggest that impedance metrics are more sensitive to changes in uterine vascular structure and function than clinically used blood flow indices and may be diagnostically useful.

Condensation

Ovine uterine vascular impedance measurements demonstrate that pregnancy causes large and small artery dilation and remodeling whereas the ovarian cycle causes only small artery dilation.

Conflict of interest

None declared.

Acknowledgements

The present study was supported in part by NIH grants HL49210, HL087144, HD38843 (RRM) and HL086939 (NCC).

References

[1] Byers MJ, Zangl A, Phernetton TM, Lopez G, Chen DB, Magness RR. Endothelial vasodilator production by ovine uterine and systemic arteries: ovarian steroid and pregnancy control of ERalpha and ERbeta levels. J Physiol 2005;565(Pt 1):85–99.
[2] Gibson TC, Phernetton TM, Wiltbank MC, Magness RR. Development and use of an ovarian synchronization model to study the effects of endogenous estrogen and nitric oxide on uterine blood flow during ovarian cycles in sheep. Biol Reprod 2004;70(6):1886–94.
[3] Magness RR, Rosenfeld CR, Carr BR. Protein kinase C in uterine and systemic arteries during ovarian cycle and pregnancy. Am J Physiol 1991;260(3 Pt 1):E464–70.
[4] Magness RR, Sullivan JA, Li Y, Phernetton TM, Bird IM. Endothelial vasodilator production by uterine and systemic arteries. VI. Ovarian and pregnancy effects on eNOS and NO(x). Am J Physiol Heart Circ Physiol 2001;280(4):H1692–8.
[5] Greiss Jr FC, Anderson SG. Uterine vescular changes during the ovarian cycle. Am J Obstet Gynecol 1969;103(5):629–40.
[6] Greiss Jr FC, Anderson SG. Effect of ovarian hormones on the uterine vascular bed. Am J Obstet Gynecol 1970;107(6):829–36.
[7] Ford SP. Control of uterine and ovarian blood flow throughout the estrous cycle and pregnancy of ewes, sows and cows. J Anim Sci 1982;55(Suppl. 2):32–42.
[8] Huckabee WE, Crenshaw C, Curet LB, Mann L, Barron DH. The effect of exogenous oestrogen on the blood flow and oxygen consumption of the uterus of the non-pregnant ewe. Q J Exp Physiol Cogn Med Sci 1970;55(1):16–24.
[9] Killam AP, Rosenfeld CR, Battaglia FC, Makowski EL, Meschia G. Effect of estrogens on the uterine blood flow of oophorectomized ewes. Am J Obstet Gynecol 1973;115(8):1045–52.
[10] Magness RR, Parker Jr CR, Rosenfeld CR. Systemic and uterine responses to chronic infusion of estradiol-17 beta. Am J Physiol 1993;265(5 Pt 1):E690–698.
[11] Magness RR, Phernetton TM, Zheng J. Systemic and uterine blood flow distribution during prolonged infusion of 17beta-estradiol. Am J Physiol 1998;275(3 Pt 2):H731–43.
[12] Magness RR, Rosenfeld CR. Local and systemic estradiol-17 beta: effects on uterine and systemic vasodilation. Am J Physiol 1989;256(4 Pt 1):E536–42.
[13] Resnik R, Brink GW, Plumer MH. The effect of progesterone on estrogen-induced uterine blood flow. Am J Obstet Gynecol 1977;128(3):251–4.
[14] Zoma W, Baker RS, Lang U, Clark KE. Hemodynamic response to tibolone in reproductive and nonreproductive tissues in the sheep. Am J Obstet Gynecol 2001;184(4):544–51.
[15] Magness RR, Phernetton TM, Gibson TC, Chen DB. Uterine blood flow responses to ICI 182 780 in ovariectomized oestradiol-17beta-treated, intact follicular and pregnant sheep. J Physiol 2005;565(Pt 1):71–83.
[16] Magness RR, Rosenfeld CR. The role of steroid hormones in the control of uterine blood flow. In: Rosenfeld CR, editor. The uterine circulation. Ithaca, NY: Perinatology Press; 1989. p. 239–71.
[17] Bruce NW. The effect of ligating a uterine artery on fetal and placental development in the rat. Biol Reprod 1976;14(3):246–7.
[18] Fuller EO, Galletti PM, Takeuchi T. Major and collateral components of blood flow to pregnant sheep uterus. Am J Physiol 1975;229(2):279–85.
[19] Palmer SK, Zamudio S, Coffin C, Parker S, Stamm E, Moore LG. Quantitative estimation of human uterine artery blood flow and pelvic blood flow redistribution in pregnancy. Obstet Gynecol 1992;80(6):1000–6.
[20] Guenther AE, Conley AJ, Van Orden DE, Farley DB, Ford SP. Structural and mechanical changes of uterine arteries during pregnancy in the pig. J Anim Sci 1988;66(12):3144–52.
[21] Hees H, Moll W, Wrobel KH, Hees I. Pregnancy-induced structural changes and trophoblastic invasion in the segmental mesometrial arteries of the guinea pig (*Cavia porcellus* L.). Placenta 1987;8(6):609–26.
[22] Mackey K, Meyer MC, Stirewalt WS, Starcher BC, McLaughlin MK. Composition and mechanics of mesenteric resistance arteries from pregnant rats. Am J Physiol 1992;263(1 Pt 2):R2–8.
[23] Osol G, Cipolla M. Interaction of myogenic and adrenergic mechanisms in isolated, pressurized uterine radial arteries from late-pregnant and nonpregnant rats. Am J Obstet Gynecol 1993;168(2):697–705.
[24] Osol G, Cipolla M. Pregnancy-induced changes in the three-dimensional mechanical properties of pressurized rat uteroplacental (radial) arteries. Am J Obstet Gynecol 1993;168(1 Pt 1):268–74.
[25] Griendling KK, Fuller EO, Cox RH. Pregnancy-induced changes in sheep uterine and carotid arteries. Am J Physiol 1985;248(5 Pt 2):H658–65.
[26] Cipolla M, Osol G. Hypertrophic and hyperplastic effects of pregnancy on the rat uterine arterial wall. Am J Obstet Gynecol 1994;171(3):805–11.
[27] Latson TW, Hunter WC, Katoh N, Sagawa K. Effect of nitroglycerin on aortic impedance, diameter, and pulse-wave velocity. Circ Res 1988;62(5):884–90.
[28] Milnor WR, Conti CR, Lewis KB, O'Rourke MF. Pulmonary arterial pulse wave velocity and impedance in man. Circ Res 1969;25(6):637–49.
[29] Zuckerman BD, Orton EC, Latham LP, Barbiere CC, Stenmark KR, Reeves JT. Pulmonary vascular impedance and wave reflections in the hypoxic calf. J Appl Physiol 1992;72(6):2118–27.
[30] Milnor TK. Characterizing harmonic immersions of surfaces with indefinite metric. Proc Natl Acad Sci USA 1982;79(6):2143–4.
[31] Saunders HM, Burns PN, Needleman L, et al. Hemodynamic factors affecting uterine artery Doppler waveform pulsatility in sheep. J Ultrasound Med 1998;17(6):357–68.
[32] Kulick LJ, Kot K, Wiltbank MC, Ginther OJ. Follicular and hormonal dynamics during the first follicular wave in heifers. Theriogenology 1999;52(5):913–21.
[33] Rosenfeld CR, Gant Jr NF. The chronically instrumental ewe: a model for studying vascular reactivity to angiotensin II in pregnancy. J Clin Invest 1981;67(2):486–92.
[34] Magness RR, Mitchell MD, Rosenfeld CR. Uteroplacental production of eicosanoids in ovine pregnancy. Prostaglandins 1990;39(1):75–88.
[35] Pant HC, Hopkinson C, Fitzpatrick RJ. Plasma oestradiol, progesterone and luteinizing hormone concentrations during the ovine oestrous cycle. J Reprod Fertil 1972;31(3):501.
[36] Alexander DP, Britton HG, Corker CS, Naftolin F, Nixon DA. Plasma luteinizing hormone and oestrogen in foetal and maternal sheep. J Endocrinol 1973;56(2):331–2.
[37] Giannattasio C, Failla M, Grappiolo A, et al. Fluctuations of radial artery distensibility throughout the menstrual cycle. Arterioscler Thromb Vasc Biol 1999;19(8):1925–9.
[38] Hayashi K, Miyachi M, Seno N, et al. Variations in carotid arterial compliance during the menstrual cycle in young women. Exp Physiol 2006;91(2):465–72.
[39] Ounis-Skali N, Mitchell GF, Solomon CG, Solomon SD, Seely EW. Changes in central arterial pressure waveforms during the normal menstrual cycle. J Investig Med 2006;54(6):321–6.
[40] Ford SP, Reynolds LP, Magness RR. Blood flow to the uterine and ovarian vascular beds of gilts during the estrous cycle or early pregnancy. Biol Reprod 1982;27(4):878–85.
[41] Rosenfeld CR, Morriss Jr FH, Battaglia FC, Makowski EL, Meschia G. Effect of estradiol-17beta on blood flow to reproductive and nonreproductive tissues in pregnant ewes. Am J Obstet Gynecol 1976;124(6):618–29.
[42] Rosenfeld CR, Killam AP, Battaglia FC, Makowski EL, Meschia G. Effect of estradiol-17, on the magnitude and distribution of uterine blood flow in nonpregnant, oophorectomized ewes. Pediatr Res 1973;7(3):139–48.
[43] Magness RR. Maternal cardiovascular and other physiologic responses to the endocrinology of pregnancy. In: The endocrinology of pregnancy. Bazer: Humana Press; 1998. pp. 507–539.
[44] Rosenfeld CR, Morriss Jr FH, Makowski EL, Meschia G, Battaglia FC. Circulatory changes in the reproductive tissues of ewes during pregnancy. Gynecol Invest 1974;5(5–6):252–68.
[45] Hayashi K, Stergiopulos N, Meister JJ, Greenwald SE, Rachev A. Techniques in the determination of the mechanial properties and constitutive laws of arterial walls. In: Leondes CT, editor. Biomechanical systems: techniques and applications. CRC Press; 2001.
[46] Burton GJ, Jauniaux E, Watson AL. Maternal arterial connections to the placental intervillous space during the first trimester of human pregnancy: the Boyd collection revisited. Am J Obstet Gynecol 1999;181(3):718–24.
[47] Grunewald C, Kublickas M, Carlstrom K, Lunell NO, Nisell H. Effects of nitroglycerin on the uterine and umbilical circulation in severe preeclampsia. Obstet Gynecol 1995;86(4 Pt 1):600–4.
[48] Hirose S, Yamada A, Kasugai M, Ishizuka T, Tomoda Y. The effect of nifedipine and dipyridamole on the Doppler blood flow waveforms of umbilical and uterine arteries in hypertensive pregnant women. Asia Oceania J Obstet Gynaecol 1992;18(2):187–93.
[49] Cobellis L, De Luca A, Pecori E, et al. Mid-trimester fetal-placental velocimetry response to nifedipine may predict early the onset of pre-eclampsia. In Vivo 2006;20(1):183–6.

[50] Cnossen JS, Morris RK, ter Riet G, et al. Use of uterine artery Doppler ultrasonography to predict pre-eclampsia and intrauterine growth restriction: a systematic review and bivariable meta-analysis. CMAJ 2008;178(6):701–11.
[51] Park YW, Cho JS, Choi HM, et al. Clinical significance of early diastolic notch depth: uterine artery Doppler velocimetry in the third trimester. Am J Obstet Gynecol 2000;182(5):1204–9.
[52] Sritippayawan S, Phupong V. Risk assessment of preeclampsia in advanced maternal age by uterine arteries Doppler at 17–21 weeks of gestation. J Med Assoc Thai 2007;90(7):1281–6.
[53] Mo LY, Bascom PA, Ritchie K, McCowan LM. A transmission line modelling approach to the interpretation of uterine Doppler waveforms. Ultrasound Med Biol 1988;14(5):365–76.
[54] Bernstein IM, Ziegler WF, Leavitt T, Badger GJ. Uterine artery hemodynamic adaptations through the menstrual cycle into early pregnancy. Obstet Gynecol 2002;99(4):620–4.
[55] Ziegler WF, Bernstein I, Badger G, Leavitt T, Cerrero ML. Regional hemodynamic adaptation during the menstrual cycle. Obstet Gynecol 1999;94(5 Pt 1):695–9.
[56] Gomez O, Figueras F, Martinez JM, et al. Sequential changes in uterine artery blood flow pattern between the first and second trimesters of gestation in relation to pregnancy outcome. Ultrasound Obstet Gynecol 2006; 28(6):802–8.
[57] Valentin L. Use of colour and spectral Doppler ultrasound examination in gynaecology. Eur J Ultrasound 1997;6(3):143–63.